Rhinovirus reduces the severity of subsequent respiratory viral infections, which is associated with dampened inflammatory responses

James T. Van Leuven[1,2], Andres J. Gonzalez[1,2], Alexander Q. Wixom[3#], John L. Clary[1,2], Benjamin J. Ridenhour[1,4], Craig R. Miller[1,2], and Tanya A. Miura[1,2*]
[1] Institute for Modeling Collaboration and Innovation, University of Idaho, Moscow, ID, USA
[2] Department of Biological Sciences, University of Idaho, Moscow, ID, USA
[3] Department of Plant Sciences, University of Idaho, Moscow, ID, USA
[4] Department of Mathematics, University of Idaho, Moscow, ID, USA

[*]Corresponding author E-mail: tmiura@uidaho.edu

[#]Current Address: Department of Gastroenterology and Hepatology, Mayo Clinic, Rochester, MN, USA

Abstract

Coinfection by unrelated viruses in the respiratory tract is common and can result in changes in disease severity compared to infection by individual virus strains. We have previously shown that inoculation of mice with rhinovirus (RV) two days prior to inoculation with a lethal dose of influenza A virus (PR8), provides complete protection against mortality. In this study, we extend that finding to a second lethal respiratory virus, pneumonia virus of mice (PVM) and characterize the differences in inflammatory responses and host gene expression in single virus infected vs. coinfected mice. RV prevented mortality and weight loss associated with PVM infection, suggesting that RV-mediated protection is more effective against PVM than PR8. Major changes in host gene expression upon PVM infection were delayed compared to PR8, which likely provides a larger time frame for RV-induced gene expression to alter the course of disease. Overall, RV induced earlier recruitment of inflammatory cells, while these populations were reduced at later times in coinfected mice. Findings common to both coinfection conditions included upregulated expression of mucin-associated genes in RV/PR8 and RV/PVM compared to mock/PR8 and mock/PVM infected mice and dampening of inflammation-related genes late

during coinfection. These findings, combined with differences in virus replication levels and disease severity, suggest that the suppression of inflammation in RV/PVM coinfected mice may be due to early suppression of viral replication, while in RV/PR8 coinfected mice may be due to a direct suppression of inflammation. Thus, a mild upper respiratory viral infection can reduce the severity of a subsequent severe viral infection in the lungs through virus-dependent mechanisms.

Author Summary

Respiratory viruses from diverse families co-circulate in human populations and are frequently detected within the same host. Though clinical studies suggest that coinfection by more than one unrelated respiratory virus may alter disease severity, animal models in which we can control the doses, timing, and strains of coinfecting viruses are critical to understand how coinfection affects disease severity. In this study, we compared gene expression and immune cell recruitment between two pairs of coinfecting viruses (RV/PR8 and RV/PVM) that both result in reduced severity compared to infection by PR8 or PVM alone in mice. Reduced disease severity was associated with suppression of inflammatory responses in the lungs. However, differences in disease kinetics and host and viral gene expression suggest that protection by coinfection with RV may be due to distinct molecular mechanisms.

Introduction

The detection of more than one virus in respiratory samples is quite common, especially among pediatric patients (1-4). There are differences in the outcomes of coinfection - whether it results in increased, decreased, or no effect on disease severity - that likely reflect different virus parings, patient populations, and study criteria. For example, coinfection with influenza B virus

55 was found to increase the severity of seasonal influenza A virus, while other virus pairings did not
56 reach statistical significance (2). Another study found increased rates of hospitalization, but not
57 other measures of clinical severity, associated with viral coinfections (1). In contrast, Martin et al.
58 found that patients with one virus detected had increased risk of severe disease than those with
59 multiple viruses detected, and some virus pairings were associated with lower viral loads in
60 coinfected patients (5). Coinfection by non-SARS-CoV-2 viruses has been detected in COVID-19
61 patients, but the impact on disease severity is not well-understood (6-8). Despite differences among
62 studies, it is clear that coinfecting viruses have the potential to alter pathogenesis and disease
63 outcomes. While clinical studies illuminate this potential, model systems in which the virus pairs,
64 doses, and timing of coinfection can be controlled are critical to understand how coinfection alters
65 pathogenesis in the respiratory tract. Therefore, we developed a mouse model using pairwise
66 combinations of respiratory viruses from different families for this purpose (9).

67 We previously found that infection of mice with a mild respiratory virus (rhinovirus strain
68 1B [RV] or mouse hepatitis virus strain 1 [MHV-1]) attenuates the severity of a subsequent
69 infection by influenza A virus (strain PR8) (9). Although coinfection does not prevent PR8
70 replication, it leads to faster viral clearance and resolution of pulmonary inflammation. Protection
71 from severe disease by viral coinfection has also been demonstrated by other groups. Similar to
72 our study, Hua et al. found that a nasal-restricted infection by MHV-1 protects mice from lethal
73 infection by PR8 and mouse-adapted severe acute respiratory syndrome coronavirus (SARS-CoV)
74 (10). Furthermore, they found that protection is associated with enhanced macrophage recruitment
75 to the lungs and up-regulation of SARS-CoV-specific CD4+ and CD8+ T cell responses (10).
76 Inhibition or delay of viral shedding also occurs in ferrets during sequential inoculations with
77 antigenically similar or dissimilar strains of influenza A and B viruses (11). A 2009 pandemic

78 influenza A (A(H1N1)pdm09) virus prevents subsequent infection of ferrets by human respiratory
79 syncytial virus (RSV) when the viruses are given within a short time frame (12). In contrast, RSV
80 does not prevent replication of A(H1N1)pdm09 in ferrets, but reduces morbidity as determined by
81 weight loss (12).

82 In this study, we aimed to evaluate whether RV-mediated disease attenuation was specific
83 to PR8, or generalizable to other respiratory viral infections. We found that RV reduced the
84 severity of an additional lethal respiratory virus, pneumonia virus of mice (PVM). PVM is a
85 relative of human RSV in the family *Pneumoviridae*, genus *Orthopneumovirus*. Infection of mice
86 with PVM results in severe disease that shares clinical features of the most severe infections by
87 RSV, including infection of the bronchiolar epithelium, granulocytic inflammation, and
88 pulmonary edema (13-15). Lethality upon infection of mice with PR8 or PVM is mediated largely
89 by dysregulated inflammatory responses, rather than overt damage due to viral replication (16-19).
90 Interestingly, there are differences in the types of immune responses that mediate protection
91 against these two viruses. Type I and III interferon (IFN) signaling and alveolar macrophages are
92 protective in PR8, but not PVM, infected mice (16, 18, 20-23). Conversely, plasmacytoid dendritic
93 cells are required for protection in PVM, but not PR8, infected mice (24, 25). Interleukin-6 (IL-6)
94 limits the severity of influenza A virus infection in mice, while it exacerbates disease in PVM-
95 infected mice (26-28). Multiple mechanisms reduce the severity of both PR8 and PVM infections,
96 including mucin production and inhibition of inflammatory responses (29-35). Based on these
97 complex differences in immunity to infection with PR8 and PVM, we used a global gene
98 expression approach combined with flow cytometry to evaluate potential mechanisms whereby
99 coinfection with RV reduces the severity of PR8 and PVM.
100

101 ## Results

102 **Coinfection with RV reduces the severity of PVM infection**

103 We previously showed that coinfection of mice with RV reduced the severity of a lethal
104 infection by influenza A virus, strain PR8 (9). Protection against lethal PR8 infection was most
105 effective when RV was given two days before PR8, but significant disease attenuation was also
106 seen when mice were inoculated with RV and PR8 concurrently. To determine if coinfection with
107 RV would attenuate disease by a second lethal respiratory viral pathogen, we inoculated mice with
108 media (mock) or RV two days before, simultaneously with, or two days after inoculation with
109 PVM. Mice were monitored daily for mortality, weight loss, and clinical signs of disease for 14
110 days after PVM inoculation.

111 Infection with PVM alone (mock/PVM) was 100% lethal with all mice succumbing to
112 infection or reaching humane endpoints by day 8 (Fig 1A). PVM-infected mice had rapid weight
113 loss (Fig 1B) and exhibited clinical signs of disease, including ruffled fur, hunched posture, labored
114 breathing, and lethargy. Mice that were inoculated with RV two days before (RV/PVM) or
115 simultaneously with (RV+PVM) PVM were completely protected from mortality (Fig 1A), weight
116 loss (Fig 1B), and clinical signs of disease. However, mice that received RV two days after PVM
117 (PVM/RV) had equivalent disease severity as mock/PVM-infected mice. Although coinfection
118 with RV reduced the severity of both PR8 (9) and PVM (Fig 1), protection was more effective
119 against PVM. Importantly, coinfection resulted in complete protection against mortality and
120 morbidity in addition to mortality when RV was given two days before or concurrent with PVM
121 (Fig 1). In contrast, RV prevented mortality, but not morbidity, when given two days before PR8
122 and giving RV and PR8 concurrently was less effective at reducing disease severity (9).

123

124 **Infection by PR8 and PVM induce different gene expression signatures in mouse lungs over**
125 **time**
126
127 To determine potential mechanisms of protection mediated by RV against PR8 and PVM,
128 we undertook a comprehensive transcriptome analysis of mouse lungs (Fig 2). Mice were
129 coinfected with RV two days before PR8 or PVM and total lung RNA was analyzed on days 0, 2,
130 4, and 6 after PR8 or PVM inoculation. Single virus-infected mice were mock-inoculated two days
131 before PR8 or PVM and total lung RNA was isolated at the same time points. Weight loss was
132 monitored daily to test for consistency with our previous morbidity and mortality analyses. RV-
133 mediated protection against PR8 was not evident by 6 days post-infection (S1 Fig) though both
134 mock/PR8 and RV/PR8 groups experienced weight loss at a rate similar to our previous study (9).
135 In contrast, complete protection against weight loss was evident in RV/PVM coinfected mice (S1
136 Fig).
137 Total lung mRNA from 3 mice per infection group and time point was collected and
138 sequenced on the Illumina platform. Of the 14.6 to 55.3 (36.4 mean) million reads obtained for
139 each sample, 83-91.2% were uniquely mapped to the mm10 mouse genome (GCA_000001635.2).
140 The expression of 24,243 and 24,421 genes were measured using Cufflinks and HTSeq,
141 respectively. We conservatively counted differentially expressed genes by requiring that they be
142 identified by Cuffdiff, EdgeR, and Deseq2 as having greater than 50% expression change and *p*-
143 values less than 0.05.
144 A principal component analysis was done with the 500 most highly variable genes to
145 visualize variation across infection groups, time points, and replicates. Most variation in host gene
146 expression was explained by the time elapsed since viral infection (Fig 3A). However, differences
147 between viruses were also apparent. Infection by PVM caused fewer gene expression changes at
148 early time points than PR8-infected mice, as seen by mock/PVM and RV/PVM day 2 samples

149 clustering closely with mock and RV day 0 samples, respectively (Fig 3A, blue and purple points).
150 By day 4, the PVM-infected mice had very different gene expression profiles than mock-
151 inoculated mice on day 0. This delayed response to PVM infection is observed in other studies
152 (16, 36). In contrast, PR8 infection dramatically altered gene expression in mice by day 2 (Fig 3A,
153 light green points). Early changes in host gene expression induced by PR8, but not PVM,
154 corresponded with earlier detection of PR8-specific transcripts (Fig 4). Moreover, the RV/PVM
155 and mock/PVM samples were very different from each other by day 4 (Fig 3A, brown points).
156 Despite dramatic differences in infection outcomes, RV/PR8 and mock/PR8 groups had similar
157 gene expression signatures until day 6 (Fig 3A, orange points). This corresponds with the similar
158 disease kinetics in these groups early during infection (9) (S1 Fig).

159 We next calculated differential gene expression levels in samples from all infected mice
160 compared to mock-inoculated mice and compared them between single virus-infected and
161 coinfected mice at each time point (Fig 3B). As reflected in the PCA, gene expression changed
162 over time, as samples taken 2 days post-infection were most similar to mock-inoculated controls
163 and samples taken 6 days post-infection were most different (Fig 3B, 3C). The transition of point
164 clustering in Fig 3B from around the origin at day 2 to spread along the 1:1 line on day 6 illustrates
165 this delayed gene expression response to viral infection. Genes differentially expressed between
166 single virus-infected and coinfected mice also displayed time-dependent clustering shifts in both
167 the PVM and PR8 experiments (Fig 3B). At 2 days post-infection, the expression values of
168 differentially expressed genes (DEGs) indicated that the coinfected samples were more different
169 from mock than the samples from single virus-infected mice (points are spread along the y-axis).
170 At 6 days post-infection, DEGs differed more between mock-inoculated and single virus-infected
171 mice than between mock-inoculated and coinfected mice (points spread along x-axis). This

172 dampening of DEGs in coinfected mice suggests that the second infection by a lethal virus is
173 ablated not only in virulence, but also in host gene expression response.

174 A summary of the numbers of DEGs across comparisons of all virus-infected to mock-
175 inoculated mice and between single virus-infected vs. coinfected mice is shown in Fig 3C and lists
176 of these DEGs are included in Supplemental Table 1. Again, the numbers of DEGs reflect the
177 delayed response to PVM infection, dampened gene expression in coinfected mice, and relative
178 similarity in gene expression in mock/PR8 and RV/PR8 infected mice.

179

180 **Viral gene expression**

181 Sequencing reads that did not map to the mouse genome were aligned with viral genomes.
182 An insignificant number of reads mapped to the RV genome. This was expected because the
183 abundance of positive-sense RV RNA and viral titers peak 24 hours after inoculation of BALB/c
184 mice (37). The earliest time we analyzed was 48 hours (day 0) after inoculation, at which point
185 RV RNA would likely represent a very low proportion of the total RNA.

186 Many reads mapped to PR8 and PVM genomes from the mice infected with these viruses
187 (Fig 4). Coinfection by RV did not prevent PR8-specific gene expression, but reads mapped to
188 PR8 were significantly lower in coinfected mice at all time points (Fig 4). Similarly, we previously
189 showed that infectious PR8 titers in the lungs were equivalent in mock/PR8 and RV/PR8 infected
190 mice on days 2 and 4 after PR8 inoculation (9). However, coinfection with RV led to earlier
191 clearance of PR8 (by day 7), corresponding with the dramatically lower PR8 mRNAs seen on day
192 6 in the present study. These findings confirm that infection with RV does not prevent subsequent
193 infection by PR8, rather it reduces viral gene expression and leads to faster clearance. Our
194 sequencing protocol only captured polyadenylated RNAs, thus these reads represent viral mRNAs

195 and not complementary (cRNA) or genomic (vRNA) viral RNAs. Based on individual gene
196 mapping, the PR8 reads predominantly mapped to the nucleoprotein (NP) and hemagglutinin (HA)
197 mRNAs (S2 Fig), which are known to be expressed at high levels during infection (38-40).

198 PVM gene expression was highest on day 4 and was robustly suppressed in RV-coinfected
199 mice (Fig 4). This suggests that RV may limit PVM infection early, which corresponds with the
200 more effective prevention of weight loss in RV/PVM (Fig 1) compared to RV/PR8 (9) coinfected
201 mice (S1 Fig). All viral genes were detected in mice infected by PVM alone (mock/PVM) on day
202 4, with the genes that express the attachment (G), nucleoprotein (N), non-structural 2 (NS2), fusion
203 (F), phosphoprotein (P), and matrix (M) proteins at the highest levels (S2 Fig). This does not
204 strictly follow the gradient of mRNA levels corresponding with gene order that is expected from
205 pneumoviruses (41), which likely reflects post-transcriptional differences in mRNA stability and
206 the heterogeneous nature of collecting cells at different stages of the virus replication cycle.

207

208 **RV induces innate immune response prior to secondary viral infection**

209 We compared gene expression in lung tissue of mock-inoculated mice to mice infected by
210 RV for 2 days (RV, day 0). Of the 24,421 genes compared, we identified 330 DEGs, of which only
211 three were down-regulated (Fig 3C and S1 Table). To get a functional picture of the RV-infected
212 lung on day 0, we identified enriched GO terms and KEGG pathways in the 330 DEGs. The most
213 highly enriched terms on this list suggest that changes in the regulation of cell cycle or cell division
214 were occurring in RV-infected compared to mock-inoculated mice; nearly all of the top 50 most
215 enriched terms involved chromosome remodeling and mitosis (S2 Table). This list of enriched
216 terms was quite different than the processes that were differentially regulated in PR8- or PVM-
217 infected mice. Up-regulation of cell division-associated genes could be occurring in epithelial cells

218 in conjunction with repair, immune cells recruited to the lungs, or both. In addition to cell division,
219 multiple immune response-related GO terms related to type I IFN signaling, chemokine signaling,
220 and immune cell chemotaxis were enriched by RV infection (S2 Table). RV infection induced up-
221 regulation of several chemokine genes, including those that recruit monocytes, neutrophils, NK
222 cells, T cells, B cells, and eosinophils (Ccl-2, 3, 6, 7, 8, 12, 17, 22, Cxcl-1, 3, 5, 9, 10, 13).
223

224 **Host gene expression changes associated with viral coinfection**

225 We next identified DEGs specific to coinfected (RV/PR8 or RV/PVM) vs. mock-
226 inoculated mice that were not differentially expressed in single virus-infected (mock/PR8 or
227 mock/PVM) vs. mock-inoculated mice at the same time points. The expression data for these three
228 gene sets (unique to RV/PR8, unique to RV/PVM, shared by RV/PR8 and RV/PVM) are provided
229 in supplemental figures (Fig S3-S5). Genes with shared up-regulation in RV-coinfected animals,
230 regardless of timepoint and second virus, included those in the mucin biosynthesis pathway, MHC
231 class II genes, and immunomodulatory genes. Genes with increased up-regulation in mice infected
232 with RV/PVM compared to mock/PVM early (days 2 and 4) included Mgl2, Ccl6, Agr2, H2-M2,
233 and Muc5b. Genes that had higher up-regulation in the single virus infections were predominantly
234 increased late (days 4 and/or 6) and included genes associated with inflammation (Angptl4) or
235 pulmonary fibrosis (Fosl2, Pappa, Sphk1). These genes were common to both PR8 and PVM
236 infections and likely result from excessive inflammation and tissue damage within the infected
237 lungs. Additional genes associated with inflammation and fibrosis (Nfkbia and Mmp9) or stress
238 responses (Hspb8, Nupr1) were reduced in RV/PVM- compared to mock/PVM-infected mice.
239 Finally, a set of genes were up-regulated in both mock/PVM- and RV/PVM-infected mice, but to

240 a higher level in mock/PVM-infected mice (S100a9, Prss22, Fga, Krt17). These genes are also
241 largely involved in inflammation and tissue damage and repair processes.

242 Genes involved in goblet cell metaplasia and mucin production were specifically increased
243 in both RV/PVM and RV/PR8 coinfections compared to the single virus-infected mice at various
244 time points. These included the major gel-forming airway mucins (Muc5ac and Muc5b), a
245 disulfide isomerase (Agr2) required for mucin folding and polymerization, and a chloride channel
246 regulator (Clca1) required for proper hydration of mucus. Additional ion channels (Slc6a20a),
247 aquaporins (Aqp9), and mucus-associated proteins (Itln1) also had increased expression in
248 coinfected mouse lungs. In addition to the mucin-related genes shared with RV/PR8, RV/PVM
249 coinfected mice had increased expression of a transcription factor (FoxA3) that promotes goblet
250 cell metaplasia and mucus production. Muc5ac and Clca1 had increased expression in coinfected
251 mice at all time points (Fig 5).

252 Based on the importance of type I IFN and inflammatory signaling pathways in the
253 pathogenesis of viral infections, we generated heatmaps demonstrating relative gene expression
254 across all groups for genes in the Hallmark Interferon Alpha Response and Inflammatory Response
255 gene sets from MSigDB (42, 43). Overall, IFN-response genes had higher expression in RV/PR8
256 vs. mock/PR8 mice on day 2 and lower expression by day 6 (Fig 6A and S6 Fig). This pattern
257 corresponds with our previous study that demonstrated increased expression of IFN-β only on day
258 2 in RV/PR8 compared to mock/PR8 infected mice (9) and also the lower PR8 gene expression in
259 coinfected mice (Fig 4). In contrast, mock/PVM and RV/PVM infected mice had delayed up-
260 regulation of IFN-response genes and mock/PVM infected mice had dramatically higher
261 expression of IFN-response genes on day 4 (Fig 6B and S6 Fig). This corresponds with the overall
262 delayed PVM-induced gene expression and reduced levels of PVM RNA in coinfected mice (Fig

263 4). RV induced expression of a small subset of IFN-response genes (Il7, Ifi27, Lamp3, Cd74, Ifi30,
264 and Lpar6) on day 0, which was maintained in RV/PVM-coinfected mice on day 2 (Fig 6B). While
265 more variation in gene expression patterns was observed in the inflammatory response gene set, a
266 large number of genes followed the same trends seen for IFN-response genes, i.e., a largely
267 dampened response in RV-coinfected mice especially at later time points (Fig 6C, 6D and S7
268 Fig). By day 6, mock/PR8-infected mice had strongly up- and down-regulated expression of
269 inflammatory response genes, while RV/PR8-coinfected mice had muted changes in expression of
270 these genes (Fig 6C). A large subset of inflammatory response genes had similar patterns as IFN-
271 response genes in mock/PVM and RV/PVM mice, including delayed expression and a muted
272 response in coinfected mice (Fig 6D). This subset includes important inducers of inflammatory
273 responses such as Nfkb1, Nfkbia, Rela, and Tlr3. Other subsets of genes (eg, Ccl17 and Ccl22)
274 had early up-regulation in RV-infected mice on day 0, which was maintained in coinfected mice
275 on day 2, and reduced in coinfected mice on days 4 and 6. In contrast with IFN-response genes,
276 subsets of inflammatory response genes had higher expression in RV/PVM compared to
277 mock/PVM infected mice throughout the course of infection. This suggests that, despite low virus
278 levels (Fig 4) and no clinical signs of disease (Fig 1) and largely muted host gene expression,
279 expression of some host genes is increased in RV/PVM-coinfected mice.
280
281 **Flow cytometry analysis**
282 Immune cells recruited to the lungs are affected by and contribute to the gene expression
283 signatures seen in whole lung tissues. To analyze differences in immune cell recruitment to the
284 lungs of single virus-infected and coinfected mice, we quantified innate immune cells in the left
285 lobes by flow cytometry at the same time points as our gene expression analyses. Total cell counts

286 from mock/PVM and RV/PVM infected mice were fairly consistent across all time points, while
287 total cells in mock/PR8 and RV/PR8 infected mice increased by day 6 (S8 Fig). CD11b+ was used
288 to differentiate leukocytes from resident lung cell populations. CD11b+ cells accounted for the
289 increase in mock/PR8 and RV/PR8 infected lungs (Fig 7A). In contrast, while CD11b+ cells
290 increased in the lungs of mice infected with mock/PVM, RV/PVM coinfected mice had reduced
291 recruitment of these cells on days 4 and 6 (Fig 7E). Neutrophils were gated based on high
292 expression of CD11b and Ly6G and the remaining cells were identified as alveolar macrophages
293 (CD64+/SiglecF+) and interstitial macrophages (CD11b+/CD64+/SiglecF-) (S8 Fig) (44, 45).
294 The proportions of neutrophils and interstitial macrophages followed the same trends as
295 total CD11b+ cells in PVM-infected mice, with lower proportions of these cells on days 4 and 6
296 in coinfected mice (Fig 7F, 7G). In contrast, interstitial macrophages were increased in RV/PVM,
297 compared to mock/PVM-infected mice, early in infection. This indicates that coinfection by RV
298 stimulates early recruitment of CD11b+ cells, specifically interstitial macrophages, while limiting
299 recruitment of inflammatory cells later in infection. PR8-infected mice had similar trends, however
300 the differences between mock/PR8 and RV/PR8 groups were less dramatic (Fig 7B, 7C).
301 Neutrophil numbers were suppressed in RV/PR8 coinfected mice compared to mock/PR8 infected
302 mice through-out the time course (Fig 7b). The interstitial macrophage proportions in mock/PR8-
303 and RV/PR8-infected mice increased over time similarly to the total CD11b+ populations (Fig
304 7C). The lower proportions of neutrophils and interstitial macrophages at later time points in RV-
305 coinfected mice corresponded with mRNA levels for chemokines. This was predominantly the
306 case for neutrophil chemokines Cxcl1 and Cxcl2 (Fig 7I, 7K) and macrophage chemokines Ccl2
307 and Ccl7 (Fig 7J, 7L). These chemokines were generally lower in RV/PR8 coinfected mice on day

308 6 and RV/PVM coinfected mice on days 4 and 6 compared to mock/PR8 and mock/PVM infected
309 mice, respectively.

310 There were no clear trends in alveolar macrophage numbers in mock/PR8- and RV/PR8-
311 infected mice (Fig 7D), though their proportions were significantly higher in RV/PVM-coinfected
312 mice compared to mock/PVM-infected mice on days 4 and 6 (Fig 7H). This is likely due to
313 depletion of alveolar macrophages by PVM infection of these cells (46). A separate flow cytometry
314 antibody panel was used to quantify CD4+ and CD8+ T cells in the lungs, but no significant
315 differences were seen between single virus-infected and coinfected mice (S9 Fig). While 6 days
316 may be too early to fully evaluate T cell responses, based on the kinetics of protection we do not
317 expect T cells to be involved.

318

319 **Discussion**

320 Previously, we found that inoculation of mice with a mild respiratory viral pathogen, RV
321 or murine coronavirus MHV-1, two days before PR8 provided significant protection against PR8-
322 mediated disease (9). In this study, we expanded these results to show that RV-mediated protection
323 was not specific to PR8, but also provided significant disease protection against a respiratory virus
324 from another viral family, PVM. This is in agreement with other studies showing protection
325 afforded by viral coinfection (10-12). Despite the commonality of coinfection resulting in reduced
326 disease severity, there are differences between the virus combinations in the kinetics of disease
327 and viral replication. Coinfection by RV provided more effective protection against PVM than
328 PR8. RV/PVM coinfected mice had little to no signs of disease (Fig 1) and significantly limited
329 PVM replication (Fig 4). In contrast, coinfection by RV prevented mortality, but not morbidity,
330 associated with PR8 infection, and reduced viral gene expression but did not prevent infection by

331 PR8 (Fig 4) (9). Further, RV given concurrently with PVM was as effective as when it was given
332 two days before PVM (Fig 1). In contrast, RV was less effective at reducing the severity of PR8
333 when given concurrently and also exacerbated disease when it was given two days after PR8 (9).
334 We also observed differences in the kinetics of gene expression in response to these virus pairs.
335 Host (Fig 3) and viral (Fig 4) gene expression changes in response to PVM were delayed compared
336 to PR8, thereby giving a larger window for RV-mediated protection. Thus, RV may be inducing
337 antiviral mechanisms that are more effective against PVM, or different mechanisms may be
338 responsible for inhibiting PVM infection and mediating effective clearance of PR8. We used
339 transcriptomic and flow cytometry analyses to identify potential mechanisms that mediate
340 protection against PR8 and PVM in mice that were coinfected with RV.

341 Analysis of RV-inoculated mice on day 0 (two days after RV inoculation) revealed up-
342 regulation of 327 genes. These genes were highly enriched in GO categories that involved cell
343 division or chemokine signaling (S2 Table). Despite expression of several chemokine and
344 chemokine receptor genes, we did not observe a dramatic increase in immune cells in the lungs of
345 RV-infected mice on day 0 (Fig 7). Although our flow cytometry results had variability in RV-
346 infected mice on day 0 between our studies, we detected a significant increase in interstitial
347 macrophages in the RV/PVM study (Fig 7G). Our flow cytometry panel was limited to focus on
348 inflammatory cells (neutrophils and macrophages) and T cells and likely missed other cell types
349 that could be recruited by RV early in infection. Further, by using whole lung for our assays, we
350 may miss populations of cells that are small, but significant, in the airways. Indeed, other studies
351 have found that neutrophils and lymphocytes are increased in the airways of RV-infected mice two
352 days after inoculation (37, 47). While the chemokine signaling genes we identified in RV-infected
353 mice on day 0 were also increased in single virus infected mice later, early upregulation of immune

354 cell recruitment in coinfected mice may contribute to early control of infection and reduced disease
355 severity.

356 In contrast to early recruitment of neutrophils, RV-coinfected mice had reduced numbers
357 of neutrophils and interstitial macrophages later during infection (Fig 7). This decrease in
358 inflammatory cell recruitment could be a result of reduced viral infection (Fig 4) and/or direct
359 down-regulation of the inflammatory response. Other studies have shown that rhinoviruses inhibit
360 macrophage responses to bacterial infection and toll-like receptor (TLR) stimulation (48, 49). This
361 down-regulation leads to reduced neutrophil recruitment and activation and results in enhanced
362 bacterial infection. While suppression of TLR signaling is detrimental during a subsequent
363 bacterial infection, it can be protective in the case of respiratory viral infections for which
364 inflammatory responses contribute to disease pathology. Blocking signaling from multiple TLRs
365 (TLR2, TLR4, TLR7, and TLR9) through inhibiting the adaptor protein TIRAP reduces the
366 severity of a lethal PR8 infection in mice (50). Inhibition of TIRAP reduces PR8-induced cytokine
367 production by macrophages and is likely protective by limiting inflammatory responses (50).
368 Similarly, inhibition of TLR2 and TLR4 signaling during PR8 infection reduces inflammatory
369 cytokine responses and disease severity (51).

370 Inflammatory responses, particularly by granulocytes, are also associated with disease
371 pathogenesis of PVM infection, independent of viral replication (32, 33). Priming with probiotic
372 bacteria or parasitic infections can reduce the severity of PVM, which corresponds with reduced
373 pulmonary inflammation. When given intranasally on days -14 and -7 prior to, or days 1 and 2
374 after PVM inoculation, *Lactobacillus spp.* prevent lethal viral infection (26, 52, 53). Bacterial
375 priming is associated with reduced production of proinflammatory cytokines and chemokines and
376 inflammatory cell recruitment to the lungs, especially neutrophils (26, 52, 53). Similarly, chronic

377 schistosomiasis protects mice from a lethal PVM infection, which corresponds with up-regulation
378 of mucus secretion pathways (30).

379 We found that coinfected mice had increased expression of several genes in the mucin
380 production pathway. Muc5ac and Clca1 had increased expression in RV-coinfected mice with PR8
381 and PVM at all time points tested (days 0, 2, 4, and 6). Muc5ac, the predominant gel-forming
382 mucin in the airways of humans and mice, is produced by goblet cells in the airway epithelium
383 and Clca1 is a chloride channel regulator that is needed for proper mucus hydration. Other studies
384 have reported up-regulation of Muc5ac mRNA and protein in the lungs and airways of RV-infected
385 mice (37, 54, 55). Influenza A virus strains, including PR8, also induce expression of Muc5ac and
386 mucus secretion (56-58). However, we only detected significant up-regulation of Muc5ac RNA in
387 mock/PR8 infected mice on day 4 and it was to a lower level than in RV/PR8 coinfected mice (Fig
388 5). While stimulation of mucus production can promote pathology in chronic airway diseases such
389 as asthma and COPD, acute mucus production in hosts with healthy airways promotes innate
390 defense against pathogen invasion. Over-expression of Muc5ac in mice has been shown to reduce
391 PR8 infection and neutrophil recruitment (31). Muc5ac also promotes neutrophil transmigration
392 and recruitment (59), thus the reduction in neutrophils seen by Ehre *et al*. may be a consequence
393 of lower viral replication. Muc5ac has also been shown to reduce the severity of PR8 and PVM
394 infections in a parasite coinfection model (30). We hypothesize that expression of Muc5ac in RV-
395 infected mice reduces infection and/or promotes more effective clearance of PR8 and PVM, which
396 results in control of excessive neutrophilic inflammation.

397 In addition, coinfected mice had increased expression of the forkhead transcription factor
398 FoxA3, which induces expression of multiple genes in the mucus production pathway that we
399 found to be concurrently upregulated, including Muc5ac, Muc5b, Agr2, and Itln1 (54). Chen et al.

400 demonstrated increased expression of FoxA3 and Muc5ac and goblet cell metaplasia in the airway
401 epithelium of mice 3 days after infection by RV (54). In contrast to upregulating expression of
402 genes associated with mucin production and goblet cell metaplasia, FoxA3 suppresses genes
403 involved in antiviral innate immune responses (54). While this would be expected to enhance viral
404 infections, early induction of antiviral immunity by coinfection may offset the inhibitory role of
405 FoxA3. Additionally, this inhibitory role may contribute to down-regulation of detrimental
406 inflammatory responses during coinfection. In addition to up-regulation of mucin genes, other
407 genes important to mucin production and hydration had increased RNA levels in coinfected mice.
408 We found dramatic differences in the effects of interferon (IFN)-response genes in PR8 vs.
409 PVM infected mice. In PVM-infected mice, increased expression of IFN-response genes was
410 delayed until day 4, at which point expression was generally lower in coinfected compared to
411 single virus infected mice. Similarly, other studies have shown no induction of IFN signaling at
412 24 hours (20) vs. strong IFN signaling by 6 days (16) after PVM infection in mice, although these
413 studies used two different PVM strains in C57Bl/6 mice. In contrast, RV/PR8 coinfected mice had
414 early (day 2) up-regulation of IFN-response genes and later down-regulation (day 6). These
415 patterns correspond to those we have seen previously in RV/PR8 coinfected mice (9), and reflect
416 a protective role of type I IFN in PR8, but not PVM, infected mice. Type I IFN signaling is
417 important for immediate antiviral defense mechanisms as well as orchestrating the correct balance
418 of immune cells responding to infection. RV/PR8 coinfected mice had early upregulation of type
419 I IFN signaling (Fig 6) without an appreciable effect on viral gene expression (Fig 4) or replication
420 (9). Indeed, others have shown that type I IFN signaling is critical for orchestrating monocyte
421 responses to PR8 infection, which in turn limits neutrophilic inflammation (18). These findings
422 demonstrate that type I IFN can provide protection during respiratory viral infections that is

423 independent of direct inhibition of viral replication. Ongoing studies to determine the role of type
424 I IFN signaling will be critical to understanding the differences in protection upon RV coinfection
425 with PR8 and PVM.
426

427 ## Materials and Methods

428 **Ethics Statement**

429 All mouse procedures were approved by the University of Idaho's Institutional Animal
430 Care and Use Committee, in compliance with the NIH Guide for the Care and Use of Laboratory
431 Animals. Female, 6-7 week-old BALB/c mice were ordered from Invivogen and were allowed to
432 acclimatize for 10 days prior to experimentation. All mice were housed in the UI Laboratory
433 Animal Research Facility under 12 hour light/dark cycles, received food and water *ad libitum*, and
434 were monitored daily for any signs of distress.
435

436 **Virus Infections**

437 Viruses used in this study include PVM strain 15 (ATCC VR-25), RV1B strain B632
438 (ATCC VR-1645) and influenza A virus, A/Puerto Rico/8/34 (H1N1; BEI Resources NR-3169).
439 Viruses were grown and titrated by $TCID_{50}$ assays in BHK-21 (PVM), HeLa (RV1B), and MDCK
440 (PR8) cell lines.

441 Mice were anesthetized using isoflurane during intranasal inoculation. RV/PVM timing
442 experiments were performed using groups of seven mice. Mice were either mock-inoculated
443 (PBS/2% FBS) or inoculated with 7.6 x 10^6 $TCID_{50}$ units of RV1B two days before,
444 simultaneously with, or two days after 1.0 x 10^4 $TCID_{50}$ units PVM in 0.05 mL intranasally. Mice
445 were then monitored daily for mortality, weight loss, and clinical signs of disease (ruffled fur,

446 hunched posture, lethargy, and labored breathing). Clinical signs in these four categories were
447 scored on a scale of 0-3 (0-none, 3-severe). Humane euthanasia was performed by overdose of
448 sodium pentobarbital followed by exsanguination when mice lost more than 25% of their starting
449 weight, exhibited severe clinical signs of disease, or at pre-determined time points. Survival and
450 weight loss data were analyzed with Prism 6.0 (Graphpad) software using Log-rank Mantel-Cox
451 and student's *t*-test corrected for multiple comparisons using the Holm-Sidak method, respectively.
452 RNA-seq and flow cytometry experiments were performed using groups of five mice. Mice
453 were either mock-inoculated (PBS/2% FBS) or inoculated with 7.6 x 10^6 $TCID_{50}$ units RV1B
454 intranasally on day -2. On day 0, mice were either inoculated with ~50 $TCID_{50}$ units of PR8 or 1.0
455 x 10^4 $TCID_{50}$ units of PVM. Mice were euthanized on days 0, 2, 4, and 6 to collect lungs for
456 analyses. Left lobes were used for flow cytometry analysis and right lobes were placed in
457 RNALater for RNA-seq analysis (see below).
458
459 **RNA-seq Analysis**
460 RNA was extracted from mouse lung tissue according to the RNeasy Plus with gDNA
461 removal protocol (QIAGEN) and quantified using an HS RNA kit and Fragment Analyzer
462 (Advanced Analytical). The three samples with the highest RNA quality from each group were
463 used for RNA-seq analysis. Stranded RNA libraries were prepared from 4 ug RNA of each sample
464 by UI's IBEST Genomics Resources Core according to KAPA's stranded mRNA-seq (KK8420)
465 library preparation protocol with capture of polyadenylated mRNAs. Libraries were tagged with
466 unique ligation adapters (BioOScientific), amplified, quantified (qubit and fragment analyzer), and
467 pooled at an equimolar ratio. The pooled library was split, pooled with other libraries, and
468 sequenced across 5 lanes of an Illumina HiSeq4000 100bp PE run at University of Oregon's

469 Genomics and Cell Characterization Core. Paired end reads (100 bp) were quality trimmed and
470 filtered using Trimmomatic v0.36 (ILLUMINACLIP:2:20:10, HEADCROP:10,
471 SLIDINGWINDOW:4:15, MINLEN:36) and mapped to the mouse genome (GRCm38/mm10
472 downloaded from UCSC) using TopHat v2.1.1 (r 300) (60, 61). The TopHat alignments were the
473 starting points for two methods of quantifying read counts and four methods of analyzing
474 differential expression. The Cufflinks v2.1.1 package (Cufflinks, Cuffmerge, Cuffdiff) was
475 compared to DE pipelines using HTSeq v0.8.0 (htseq-count -m intersection -nonempty -s reverse
476 -t exon) followed by DESeq2 v1.18.1, and EdgeR 3.18.1 (62, 63). DESeq2 and EdgeR were run
477 within the SARTools wrapper (64). DEGs with adjusted p values below 0.05 were dropped. A text
478 file containing important parameters and code is included in S1 File.

479 *Analysis of viral gene expression*

480 Reads that did not map to the mouse genome were extracted and de-interleaved using
481 BBmaps' reformat script (http://sourceforge.net/projects/bbmap/) to give pair reads for mapping.
482 These reads were aligned to the RV1B (D00239), PR8 (LC120388-LC120395), and PVM
483 (AY729016) genomes using TopHat v2.1.1 and gene coverages were counted using HTseq v0.8.0
484 (see parameters above). Statistics were performed using a generalized linear model in R.

485 *DEG function analysis*

486 The DEG lists for each treatment comparison were searched for differentially enriched
487 gene ontologies (GO terms) and KEGG pathways using CompGO (65). CompGO utilizes gene
488 expression level data (as opposed to just gene names) to identify potential functions that differ
489 between treatments. We ran CompGO on DEG lists from each individual method (Cufflinks,
490 EdgeR, DESeq2) and combinations of gene sets to anecdotally look for consistency across
491 methods.

492

493 **Flow Cytometry**

494 The left lung lobe of each sample was dissociated in RPMI medium containing type IV
495 collagenase (MP Biomedicals) and DNase I (Spectrum) using gentleMACS C tubes according to
496 the manufacturer's recommendations (Miltenyi Biotec). Cells were filtered through a 70 μm
497 strainer and red blood cells were lysed before blocking F_C receptors using anti-CD16/CD32
498 (BioLegend). Cell-specific proteins were labeled with the following antibodies: CD11b-Alexa
499 Fluor 488 (eBiosciences), Ly6G-APC (eBiosciences), CD64-PE (BioLegend), SiglecF-PerCP-
500 Cy5.5 (BD Biosciences), or the appropriate isotype control antibodies. Stained cells were
501 incubated in BD Stabilizing Fixative (BD Biosciences) and analyzed using a FACS Aria
502 Cytometer (BD Biosciences). Results were analyzed using FlowJo software (Treestar) and gating
503 was performed based on fluorescence minus one controls. The gating strategy used to identify
504 neutrophils, alveolar macrophages, and interstitial macrophages is shown in S8 Fig.

505

506 **Statistical Analysis**

507 We analyzed flow cytometry (Fig 7) and viral read count (Fig 4) data resulting from our
508 experiments to identify time-varying differences between mice infected with PR8 or PVM alone
509 or coinfected with RV. To this end, we used negative binomial regression on each response
510 variable with an explanatory model that had a main effect of days post-infections, a main effect of
511 treatment (single or coinfection), and the interaction between the two main effects. Response
512 variables were the number of CD11b cells, neutrophils, interstitial macrophages, alveolar
513 macrophages, and viral read counts; all response variables were normalized versus total cell count
514 except for viral RNA read count which was normalized against total RNA read count. Due to *a*

515 *prior* visual investigation of our data, it seemed some of our response variables might be better fit
516 with a quadratic time term. Because of this we fit an alternative model that included an orthogonal
517 polynomial of degree 2 for time. We assessed whether the quadratic model was better than the
518 linear model using a likelihood ratio test and chose the quadratic model if it offered a significant
519 improvement in fit over the simpler linear model. The significance of treatment and time was
520 determined using a type-I ANOVA. To detect differences between treatments at a given time, we
521 also performed *post hoc* pairwise comparisons of the modeled mean at our observational time
522 points (days 0, 2, 4, and 6) using the emmeans package in R. Supplemental Table 3 provides
523 information on the analyses, including which time model was used, the significance of treatment
524 and time. Significant contrasts are shown in individual figures.
525
526 **Data availability**
527 Raw Illumina reads have been deposited in NCBI SRA database under accession numbers
528 SRR7060120-SRR7060117 under project PRJNA453386.
529
530
531 ## Acknowledgements
532 This study was supported by the National Institutes of Health (NIH) grants P20 GM104420
533 and P20 GM103397. We thank the Institute for Bioinformatic and Evolutionary Studies (IBEST)
534 Genomics Resources Core and Optical Imaging Core. The following reagents were obtained
535 through the NIH Biodefense and Emerging Infections Research Resources Repository, NIAID,
536 NIH: Influenza A Virus, A/Puerto Rico/8/34 (H1N1).
537

538 **References**

539 1. Cilla G, Onate E, Perez-Yarza EG, Montes M, Vicente D, Perez-Trallero E. Viruses in
540 community-acquired pneumonia in children aged less than 3 years old: High rate of viral
541 coinfection. Journal of Medical Virology. 2008;80(10):1843-9.
542 2. Goka E, Vallely P, Mutton K, Klapper P. Influenza A viruses dual and multiple infections
543 with other respiratory viruses and risk of hospitalisation and mortality. Influenza Other Respir
544 Viruses. 2013;7(6):1079-87.
545 3. Nolan VG, Arnold SR, Bramley AM, Ampofo K, Williams DJ, Grijalva CG, et al. Etiology
546 and Impact of Coinfections in Children Hospitalized With Community-Acquired Pneumonia. J
547 Infect Dis. 2018;218(2):179-88.
548 4. Xia W, Shao J, Guo Y, Peng X, Li Z, Hu D. Clinical and CT features in pediatric patients
549 with COVID-19 infection: Different points from adults. Pediatr Pulmonol. 2020;55(5):1169-74.
550 5. Martin ET, Kuypers J, Wald A, Englund JA. Multiple versus single virus respiratory
551 infections: viral load and clinical disease severity in hospitalized children. Influenza and other
552 respiratory viruses. 2012;6(1):71-7.
553 6. Kim D, Quinn J, Pinsky B, Shah NH, Brown I. Rates of co-infection between SARS-CoV-2
554 and other respiratory pathogens. JAMA. 2020;323(20):2085-6.
555 7. Li Z, Chen Zm, Y LDC, Zhan aQ, Li SQ, Cheng J, et al. Coinfection with SARS-CoV-2
556 and other respiratory pathogens in patients with COVID-19 in Guangzhou, China. Journal of
557 Medical Virology. 2020;92(11):2381-3.
558 8. Lansbury L, Lim B, Baskaran V, Lim WS. Co-infections in people with COVID-19: a
559 systematic review and meta-analysis. Journal of Infection. 2020;81(2):266-75.
560 9. Gonzalez AJ, Ijezie EC, Balemba OB, Miura TA. Attenuation of Influenza A Virus Disease
561 Severity by Viral Coinfection in a Mouse Model. J Virol. 2018;92(23):pii: e00881-18.
562 10. Hua X, Vijay R, Channappanavar R, Athmer J, Meyerholz DK, Pagedar N, et al. Nasal
563 priming by a murine coronavirus provides protective immunity against lethal heterologous virus
564 pneumonia. JCI Insight. 2018;3(11).
565 11. Laurie KL, Guarnaccia TA, Carolan LA, Yan AW, Aban M, Petrie S, et al. Interval
566 Between Infections and Viral Hierarchy Are Determinants of Viral Interference Following
567 Influenza Virus Infection in a Ferret Model. J Infect Dis. 2015;212(11):1701-10.
568 12. Chan KF, Carolan LA, Korenkov D, Druce J, McCaw J, Reading PC, et al. Investigating
569 Viral Interference Between Influenza A Virus and Human Respiratory Syncytial Virus in a Ferret
570 Model of Infection. J Infect Dis. 2018;218(3):406-17.
571 13. Dyer KD, Garcia-Crespo KE, Glineur S, Domachowske JB, Rosenberg HF. The
572 Pneumonia Virus of Mice (PVM) model of acute respiratory infection. Viruses. 2012;4(12):3494-
573 510.
574 14. Easton AJ, Domachowske JB, Rosenberg HF. Animal pneumoviruses: molecular genetics
575 and pathogenesis. Clin Microbiol Rev. 2004;17(2):390-412.
576 15. Habibi MS, Thwaites RS, Chang M, Jozwik A, Paras A, Kirsebom F, et al. Neutrophilic
577 inflammation in the respiratory mucosa predisposes to RSV infection. Science.
578 2020;370(6513):eaba9301.
579 16. Garvey TL, Dyer KD, Ellis JA, Bonville CA, Foster B, Prussin C, et al. Inflammatory
580 responses to pneumovirus infection in IFN-alpha beta R gene-deleted mice. J Immunol.
581 2005;175(7):4735-44.

582 17. Walsh KB, Teijaro JR, Brock LG, Fremgen DM, Collins PL, Rosen H, et al. Animal model
583 of respiratory syncytial virus: CD8+ T cells cause a cytokine storm that is chemically tractable by
584 sphingosine-1-phosphate 1 receptor agonist therapy. J Virol. 2014;88(11):6281-93.
585 18. Seo SU, Kwon HJ, Ko HJ, Byun YH, Seong BL, Uematsu S, et al. Type I interferon
586 signaling regulates Ly6C(hi) monocytes and neutrophils during acute viral pneumonia in mice.
587 PLoS Pathog. 2011;7(2):e1001304.
588 19. Stifter SA, Bhattacharyya N, Pillay R, Florido M, Triccas JA, Britton WJ, et al. Functional
589 Interplay between Type I and II Interferons Is Essential to Limit Influenza A Virus-Induced Tissue
590 Inflammation. PLoS Pathog. 2016;12(1):e1005378.
591 20. Heinze B, Frey S, Mordstein M, Schmitt-Graff A, Ehl S, Buchholz UJ, et al. Both
592 nonstructural proteins NS1 and NS2 of pneumonia virus of mice are inhibitors of the interferon
593 type I and type III responses in vivo. J Virol. 2011;85(9):4071-84.
594 21. Mordstein M, Kochs G, Dumoutier L, Renauld JC, Paludan SR, Klucher K, et al.
595 Interferon-lambda contributes to innate immunity of mice against influenza A virus but not against
596 hepatotropic viruses. PLoS Pathog. 2008;4(9):e1000151.
597 22. Rigaux P, Killoran KE, Qiu Z, Rosenberg HF. Depletion of alveolar macrophages prolongs
598 survival in response to acute pneumovirus infection. Virology. 2011.
599 23. Cardani A, Boulton A, Kim TS, Braciale TJ. Alveolar Macrophages Prevent Lethal
600 Influenza Pneumonia By Inhibiting Infection Of Type-1 Alveolar Epithelial Cells. PLoS Pathog.
601 2017;13(1):e1006140.
602 24. Davidson S, Kaiko G, Loh Z, Lalwani A, Zhang V, Spann K, et al. Plasmacytoid dendritic
603 cells promote host defense against acute pneumovirus infection via the TLR7-MyD88-dependent
604 signaling pathway. J Immunol. 2011;186(10):5938-48.
605 25. Wolf AI, Buehler D, Hensley SE, Cavanagh LL, Wherry EJ, Kastner P, et al. Plasmacytoid
606 dendritic cells are dispensable during primary influenza virus infection. J Immunol.
607 2009;182(2):871-9.
608 26. Percopo CM, Ma M, Brenner TA, Krumholz JO, Break TJ, Laky K, et al. Critical Adverse
609 Impact of IL-6 in Acute Pneumovirus Infection. J Immunol. 2019;202(3):871-82.
610 27. Pyle CJ, Uwadiae FI, Swieboda DP, Harker JA. Early IL-6 signalling promotes IL-27
611 dependent maturation of regulatory T cells in the lungs and resolution of viral immunopathology.
612 PLoS Pathog. 2017;13(9):e1006640.
613 28. Yang ML, Wang CT, Yang SJ, Leu CH, Chen SH, Wu CL, et al. IL-6 ameliorates acute
614 lung injury in influenza virus infection. Sci Rep. 2017;7:43829.
615 29. Martinez EC, Garg R, Shrivastava P, Gomis S, van Drunen Littel-van den Hurk S.
616 Intranasal treatment with a novel immunomodulator mediates innate immune protection against
617 lethal pneumonia virus of mice. Antiviral Res. 2016;135:108-19.
618 30. Scheer S, Krempl C, Kallfass C, Frey S, Jakob T, Mouahid G, et al. S. mansoni bolsters
619 anti-viral immunity in the murine respiratory tract. PLoS One. 2014;9(11):e112469.
620 31. Ehre C, Worthington EN, Liesman RM, Grubb BR, Barbier D, O'Neal WK, et al.
621 Overexpressing mouse model demonstrates the protective role of Muc5ac in the lungs. Proc Natl
622 Acad Sci U S A. 2012;109(41):16528-33.
623 32. Bonville CA, Easton AJ, Rosenberg HF, Domachowske JB. Altered pathogenesis of severe
624 pneumovirus infection in response to combined antiviral and specific immunomodulatory agents.
625 J Virol. 2003;77(2):1237-44.

626 33. Bonville CA, Lau VK, DeLeon JM, Gao JL, Easton AJ, Rosenberg HF, et al. Functional
627 antagonism of chemokine receptor CCR1 reduces mortality in acute pneumovirus infection in
628 vivo. J Virol. 2004;78(15):7984-9.
629 34. Lin KL, Sweeney S, Kang BD, Ramsburg E, Gunn MD. CCR2-antagonist prophylaxis
630 reduces pulmonary immune pathology and markedly improves survival during influenza infection.
631 J Immunol. 2011;186(1):508-15.
632 35. Ichikawa A, Kuba K, Morita M, Chida S, Tezuka H, Hara H, et al. CXCL10-CXCR3
633 enhances the development of neutrophil-mediated fulminant lung injury of viral and nonviral
634 origin. Am J Respir Crit Care Med. 2013;187(1):65-77.
635 36. Buchholz UJ, Ward JM, Lamirande EW, Heinze B, Krempl CD, Collins PL. Deletion of
636 nonstructural proteins NS1 and NS2 from pneumonia virus of mice attenuates viral replication and
637 reduces pulmonary cytokine expression and disease. J Virol. 2009;83(4):1969-80.
638 37. Bartlett NW, Walton RP, Edwards MR, Aniscenko J, Caramori G, Zhu J, et al. Mouse
639 models of rhinovirus-induced disease and exacerbation of allergic airway inflammation. Nat Med.
640 2008;14(2):199-204.
641 38. Kebaabetswe LP, Haick AK, Gritsenko MA, Fillmore TL, Chu RK, Purvine SO, et al.
642 Proteomic analysis reveals down-regulation of surfactant protein B in murine type II pneumocytes
643 infected with influenza A virus. Virology. 2015;483:96-107.
644 39. Kummer S, Flottmann M, Schwanhausser B, Sieben C, Veit M, Selbach M, et al. Alteration
645 of protein levels during influenza virus H1N1 infection in host cells: a proteomic survey of host
646 and virus reveals differential dynamics. PLoS One. 2014;9(4):e94257.
647 40. Fabozzi G, Oler AJ, Liu P, Chen Y, Mindaye S, Dolan MA, et al. Strand-Specific Dual
648 RNA Sequencing of Bronchial Epithelial Cells Infected with Influenza A/H3N2 Viruses Reveals
649 Splicing of Gene Segment 6 and Novel Host-Virus Interactions. J Virol. 2018;92(17).
650 41. Collins PL, Fearns R, Graham BS. Respiratory syncytial virus: virology, reverse genetics,
651 and pathogenesis of disease. Curr Top Microbiol Immunol. 2013;372:3-38.
652 42. Subramanian A, Tamayo P, Mootha VK, Mukherjee S, Ebert BL, Gillette MA, et al. Gene
653 set enrichment analysis: a knowledge-based approach for interpreting genome-wide expression
654 profiles. Proc Natl Acad Sci U S A. 2005;102(43):15545-50.
655 43. Liberzon A, Birger C, Thorvaldsdottir H, Ghandi M, Mesirov JP, Tamayo P. The
656 Molecular Signatures Database (MSigDB) hallmark gene set collection. Cell Syst. 2015;1(6):417-
657 25.
658 44. Misharin AV, Morales-Nebreda L, Mutlu GM, Budinger GR, Perlman H. Flow cytometric
659 analysis of macrophages and dendritic cell subsets in the mouse lung. Am J Respir Cell Mol Biol.
660 2013;49(4):503-10.
661 45. Gibbings SL, Thomas SM, Atif SM, McCubbrey AL, Desch AN, Danhorn T, et al. Three
662 Unique Interstitial Macrophages in the Murine Lung at Steady State. Am J Respir Cell Mol Biol.
663 2017;57(1):66-76.
664 46. Dyer KD, Drummond RA, Rice TA, Percopo CM, Brenner TA, Barisas DA, et al. Priming
665 of the Respiratory Tract with Immunobiotic Lactobacillus plantarum Limits Infection of Alveolar
666 Macrophages with Recombinant Pneumonia Virus of Mice (rK2-PVM). J Virol. 2015;90(2):979-
667 91.
668 47. Ganesan S, Pham D, Jing Y, Farazuddin M, Hudy MH, Unger B, et al. TLR2 Activation
669 Limits Rhinovirus-Stimulated CXCL-10 by Attenuating IRAK-1-Dependent IL-33 Receptor
670 Signaling in Human Bronchial Epithelial Cells. J Immunol. 2016;197(6):2409-20.

671 48. Unger BL, Faris AN, Ganesan S, Comstock AT, Hershenson MB, Sajjan US. Rhinovirus
672 attenuates non-typeable Hemophilus influenzae-stimulated IL-8 responses via TLR2-dependent
673 degradation of IRAK-1. PLoS Pathog. 2012;8(10):e1002969.
674 49. Oliver BG, Lim S, Wark P, Laza-Stanca V, King N, Black JL, et al. Rhinovirus exposure
675 impairs immune responses to bacterial products in human alveolar macrophages. Thorax.
676 2008;63(6):519-25.
677 50. Piao W, Shirey KA, Ru LW, Lai W, Szmacinski H, Snyder GA, et al. A Decoy Peptide
678 that Disrupts TIRAP Recruitment to TLRs Is Protective in a Murine Model of Influenza. Cell Rep.
679 2015;11(12):1941-52.
680 51. Prantner D, Shirey KA, Lai W, Lu W, Cole AM, Vogel SN, et al. The theta-defensin
681 retrocyclin 101 inhibits TLR4- and TLR2-dependent signaling and protects mice against influenza
682 infection. J Leukoc Biol. 2017;102(4):1103-13.
683 52. Gabryszewski SJ, Bachar O, Dyer KD, Percopo CM, Killoran KE, Domachowske JB, et
684 al. Lactobacillus-mediated priming of the respiratory mucosa protects against lethal pneumovirus
685 infection. J Immunol. 2011;186(2):1151-61.
686 53. Percopo CM, Rice TA, Brenner TA, Dyer KD, Luo JL, Kanakabandi K, et al.
687 Immunobiotic Lactobacillus administered post-exposure averts the lethal sequelae of respiratory
688 virus infection. Antiviral Res. 2015;121:109-19.
689 54. Chen G, Korfhagen TR, Karp CL, Impey S, Xu Y, Randell SH, et al. Foxa3 induces goblet
690 cell metaplasia and inhibits innate antiviral immunity. Am J Respir Crit Care Med.
691 2014;189(3):301-13.
692 55. Zhu L, Lee PK, Lee WM, Zhao Y, Yu D, Chen Y. Rhinovirus-induced major airway mucin
693 production involves a novel TLR3-EGFR-dependent pathway. Am J Respir Cell Mol Biol.
694 2009;40(5):610-9.
695 56. Barbier D, Garcia-Verdugo I, Pothlichet J, Khazen R, Descamps D, Rousseau K, et al.
696 Influenza A induces the major secreted airway mucin MUC5AC in a protease-EGFR-extracellular
697 regulated kinase-Sp1-dependent pathway. Am J Respir Cell Mol Biol. 2012;47(2):149-57.
698 57. Siegel SJ, Roche AM, Weiser JN. Influenza promotes pneumococcal growth during
699 coinfection by providing host sialylated substrates as a nutrient source. Cell Host Microbe.
700 2014;16(1):55-67.
701 58. Buchweitz JP, Harkema JR, Kaminski NE. Time-dependent airway epithelial and
702 inflammatory cell responses induced by influenza virus A/PR/8/34 in C57BL/6 mice. Toxicol
703 Pathol. 2007;35(3):424-35.
704 59. Koeppen M, McNamee EN, Brodsky KS, Aherne CM, Faigle M, Downey GP, et al.
705 Detrimental role of the airway mucin Muc5ac during ventilator-induced lung injury. Mucosal
706 Immunol. 2013;6(4):762-75.
707 60. Bolger AM, Lohse M, Usadel B. Trimmomatic: a flexible trimmer for Illumina sequence
708 data. Bioinformatics. 2014;30(15):2114-20.
709 61. Kim D, Pertea G, Trapnell C, Pimentel H, Kelley R, Salzberg S. TopHat2: accurate
710 alignment of transcriptomes in the presence of insertions, deletions and gene fusions. Genome
711 Biol. 2013;14(4).
712 62. Trapnell C, Williams B, Pertea G, Mortazavi A, Kwan G, Baren Jv, et al. Transcript
713 assembly and quantification by RNA-Seq reveals unannotated transcripts and isoform switching
714 during cell differentiation. Nature Biotechnology. 2010.
715 63. Anders S, Pyl PT, Huber W. HTSeq—a Python framework to work with high-throughput
716 sequencing data. Bioinformatics. 2015;31(2):166-9.

717 64. Varet H, Brillet-Guéguen L, Coppee J-Y, Dillies M-A. SARTools: A DESeq2- and EdgeR-
718 Based R Pipeline for Comprehensive Differential Analysis of RNA-Seq Data. PLoS One. 2016.
719 65. Waardenberg AJ, Bassett SD, Bouveret R, Harvey RP. CompGO: an R package for
720 comparing and visualizing Gene Ontology enrichment differences between DNA binding
721 experiments. BMC Bioinformatics. 2015;16:275.
722

723

724 Supporting Information

725 **Supplemental Table 1** provides raw read counts (mean of the three replicates and normalized to
726 library size) and log2 fold change values for genes that had statistically significant differences in
727 expression between each comparison (infected or coinfected vs. mock-inoculated and coinfected
728 vs. single infected).

729

730 **Supplemental Table 2** provides statistically significant GO terms for each comparison (infected
731 or coinfected vs. mock-inoculated and coinfected vs. single infected).

732

733 **Supplemental Table 3** provides a summary of results from negative binomial regression analyses
734 of flow cytometry and viral read count data.

735

736 **S1 Fig. Weight loss of mice used in the RNA-seq and flow cytometry experiments.** Mice were
737 inoculated intranasally with saline (mock) or RV on day -2 and PR8 or PVM on day 0. Weight
738 was recorded daily for all mice until the pre-determined time points. Days -2 through 2, N=15 per
739 group; days 3 through 4, N=10 per group; days 5 through 6, N= 5 per group.

740

741 **S2 Fig. Read coverage of individual viral genes.** The proportion of reads mapping to each viral
742 gene is shown for mice infected with PR8 or PVM.

743

744 **S3 Fig. Heatmap of mock/PR8 vs. RV/PR8 unique genes.** Expression of genes that are
745 significantly different between mock/PR8 and RV/PR8 infected mice that are not significant
746 between mock/PVM and RV/PVM infected mice. Colors represent Z-scores for individual genes
747 across infections and time points as described for Fig 6.

748

749 **S4 Fig. Heatmap of mock/PVM vs. RV/PVM unique genes.** Expression of genes that are
750 significantly different between mock/PVM and RV/PVM infected mice that are not significant
751 between mock/PR8 and RV/PR8 infected mice. Colors represent Z-scores for individual genes
752 across infections and time points as described for Fig 6.

753

754 **S5 Fig. Heatmap of differentially expressed genes shared by coinfected mice.** Expression of
755 genes that are significantly different between mock/PVM and RV/PVM infected mice that are also
756 significant between mock/PR8 and RV/PR8 infected mice. Colors represent Z-scores for
757 individual genes across infections and time points as described for Fig 6.

758

759 **S6 Fig. Heatmaps of MSigDB Hallmark Interferon Alpha Response gene set shown in Figure**
760 **6, including gene names.** See Fig 6 legend for details.

761

762 **S7 Fig. Heatmaps of MSigDB Hallmark Inflammatory Response gene set shown in Figure 6,**
763 **including gene names.** See Fig 6 legend for details.

764

765 **S8 Fig. Total cell counts and gating strategy for flow cytometry.** Left lungs were processed for
766 flow cytometry staining with antibodies against CD11b, Ly6G, CD64, and Siglec F. Total cell
767 counts for all samples and representative plots showing the gating strategy to identify neutrophils,
768 alveolar macrophages, and interstitial macrophages are shown.
769
770 **S9 Fig. CD4 and CD8 cell counts by flow cytometry.** Left lungs were processed for flow
771 cytometry staining with antibodies against CD3, CD4, and CD8 to identify total CD4+ and CD8+
772 T cells.
773
774

775 Figure Legends

776 **Fig 1. Coinfection with RV reduces the severity of PVM infection.** Groups of 7 BALB/c mice
777 were either mock-inoculated (mock/PVM) or inoculated intranasally with 7.6 x 10^6 $TCID_{50}$ units
778 of RV two days before (RV/PVM), simultaneously with (RV+PVM), or two days after (PVM/RV)
779 1.0x10^4 $TCID_{50}$ units of PVM. Mice were monitored daily for (A) mortality and (B) weight loss.
780 Statistical significance compared to mock/PVM was determined by (A) Log-rank Mantel-Cox test
781 and (B) student's t-test corrected for multiple comparisons using the Holm-Sidak method. P-value
782 *$p \leq 0.05$, **$p \leq 0.001$.
783
784 **Fig 2**. **Experimental outline of transcriptome study.** Mice were inoculated with RV or saline
785 (mock) two days before challenge with PR8 or PVM. RNA was extracted from lung tissue from
786 three mice per group on day 0 for mock and RV treated controls and days 2, 4, and 6 for mice
787 receiving PR8 or PVM on day 0 and analyzed by RNA-seq.

788

789 **Fig 3. Patterns of mouse gene expression in lungs upon infection and coinfection.** (A) Principal
790 component analysis of RNA-seq data shows that the greatest variance in gene expression is
791 primarily due to time since infection. The largest distances in single vs. coinfected groups are
792 mock/PVM vs. RV/PVM on day 4 and mock/PR8 vs. RV/PR8 on day 6. (B) The scatter plots show
793 the log2 fold change values of all genes compared to mock-inoculated mice on day 0. Genes
794 upregulated in the coinfected compared to the single-virus infected mice are colored green. Down-
795 regulated genes are colored purple. (C) Numbers of DEGs in all pairwise comparisons. The
796 number of genes upregulated in the infected (versus mock) or coinfected (versus mock or single)
797 mice are shown in green. Downregulated genes are shown in purple. See Supplemental Table 1
798 for lists of gene names and log2 fold change values.

799

800 **Fig 4. Viral gene expression in single virus and coinfected mouse lungs.** For each group, the
801 three replicates are shown with box plots indicating the quantile values of percent non-mouse reads
802 mapped to viral genomes. Asterisks indicate significantly different treatment pairs, see
803 Supplemental Table 3. P-value *$p<0.05$, **$p<0.01$, ***$p\leq0.001$.

804

805 **Fig 5. Mucin-related genes have increased expression in RV coinfected mice across all time**
806 **points.** Log2 fold change values compared to mock day 0 are shown for mucin 5ac (Muc5ac) and
807 chloride channel accessory 1 (Clca1) genes, which are required for mucus production and
808 hydration, respectively.

809

810 **Fig 6. Expression of MSigDB Hallmark Interferon Alpha Response and Inflammatory**
811 **Response gene sets.** Heatmaps of Hallmark Interferon Alpha Response genes showing the relative
812 expression (Z-scores) of genes for the (A) PR8 or (B) PVM coinfection RNA-seq timecourse.
813 Heatmaps of Hallmark Inflammatory Response genes showing the relative expression (Z-scores)
814 of genes for the (C) PR8 or (D) PVM coinfection RNA-seq timecourse. All heatmaps represent
815 DESeq2 normalized counts where each gene is a row and each is ordered individually by
816 hierarchical clustering. The colors (blue < white < red) represent the Z-score and a more intense
817 color indicates a lower (blue) or higher (red) relative expression of that gene in that condition.
818 Fully labeled heatmaps can be found in S6 and S7 Fig.
819
820 **Fig 7. Flow cytometry analysis of innate immune cell populations in the lungs upon viral**
821 **infection and coinfection.** Mice were inoculated with mock or RV on day -2 and PR8 (A-D) or
822 PVM (E-H) on day 0, followed by analysis of specific cell populations in lung homogenates by
823 flow cytometry, including total CD11b+ cell counts (A, E), and percentages of $CD11b^{hi}/Ly6G^{hi}$
824 neutrophils (B, F), CD11b+/CD64+/SiglecF-/Ly6G- interstitial macrophages (C, B), and
825 CD64+/SiglecF+/Ly6G- alveolar macrophages (D, H). Asterisks indicate significantly different
826 treatment pairs, see Supplemental Table 3. P-value *$p<0.05$, **$p<0.01$, ***$p\leq0.001$. Expression
827 of neutrophil (I, K) and monocyte/macrophage (J, L) specific chemokine genes from the RNA-seq
828 analysis are shown as Log2 fold change vs. mock-inoculated mice.

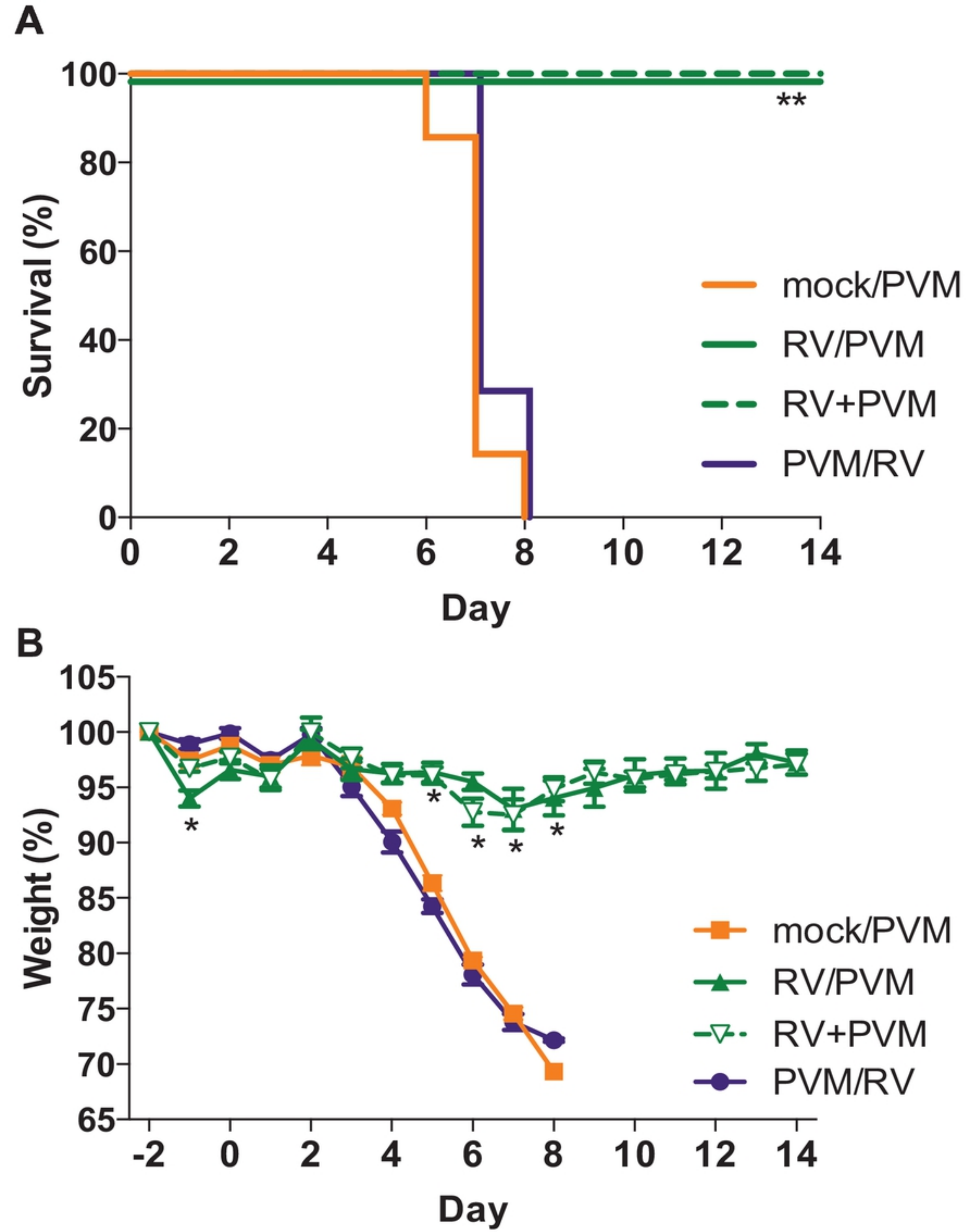
A
100
80
60
40
20
0
Survival (%)
**
mock/PVM
RV/PVM
RV+PVM
PVM/RV
0
2
4
6
8
10
12
14
Day
B
105
100
95
90
85
80
75
70
65
Weight (%)
*
*
*
*
*
mock/PVM
RV/PVM
RV+PVM
PVM/RV
-2
0
2
4
6
8
10
12
14
Day

Fig 1

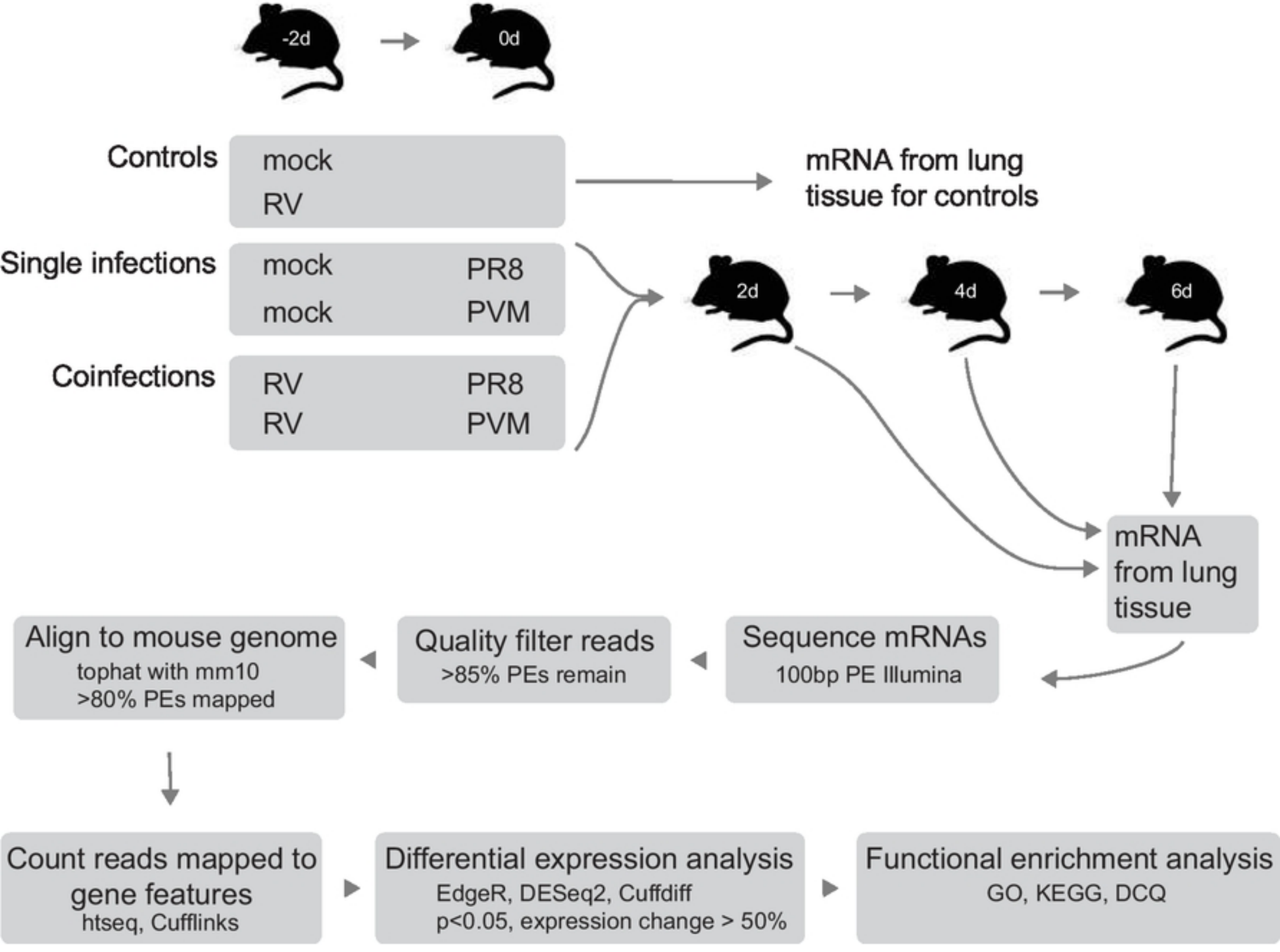
-2d
0d
Controls
mock
RV
mRNA from lung tissue for controls
Single infections
mock
PR8
mock
PVM
Coinfections
RV
PR8
RV
PVM
2d
4d
6d
mRNA from lung tissue
Align to mouse genome
tophat with mm10
>80% PEs mapped
Quality filter reads
>85% PEs remain
Sequence mRNAs
100bp PE Illumina
Count reads mapped to gene features
htseq, Cufflinks
Differential expression analysis
EdgeR, DESeq2, Cuffdiff
p<0.05, expression change > 50%
Functional enrichment analysis
GO, KEGG, DCQ

Fig 2

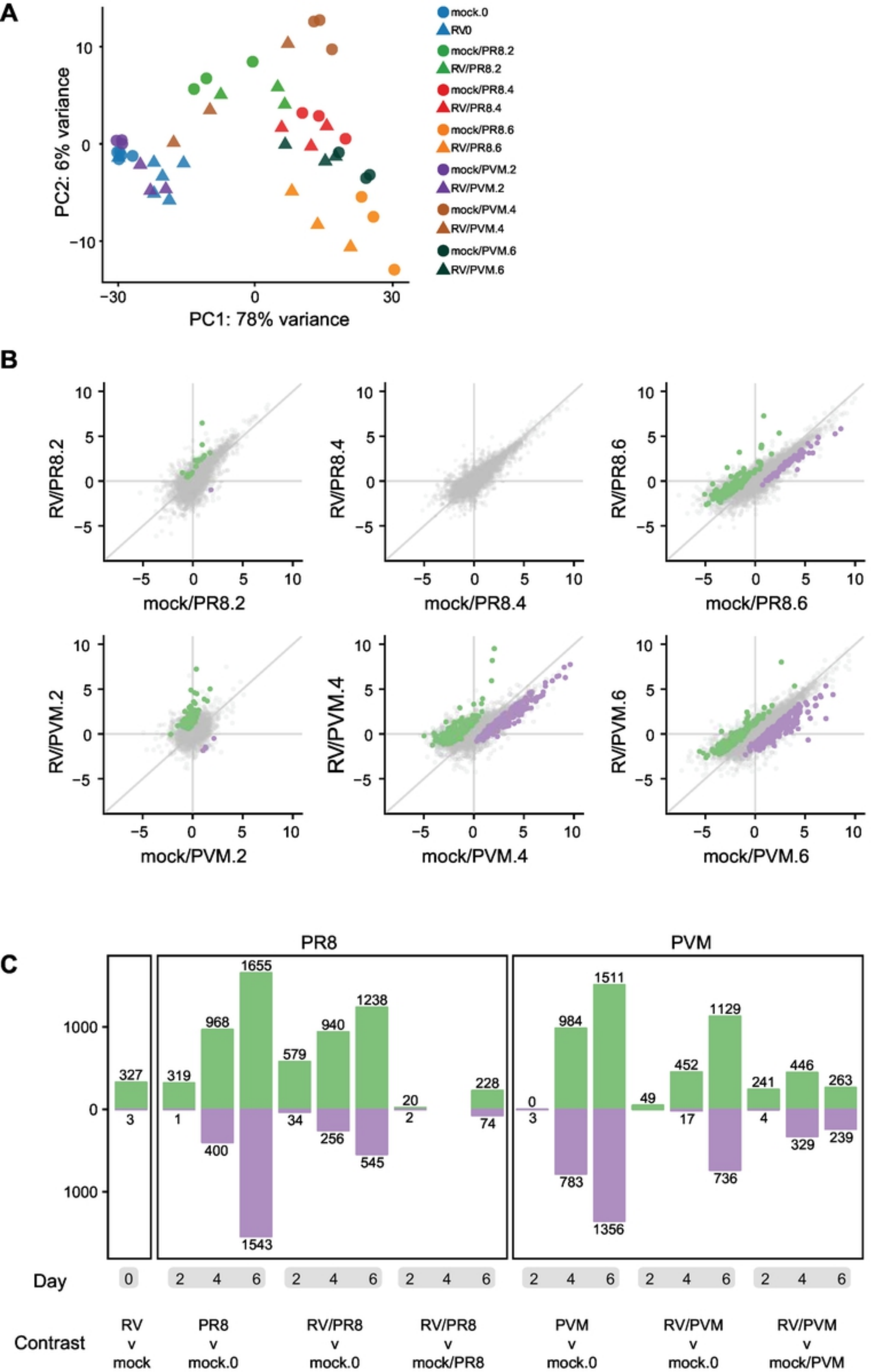
A
PC2: 6% variance
PC1: 78% variance
mock.0
RV0
mock/PR8.2
RV/PR8.2
mock/PR8.4
RV/PR8.4
mock/PR8.6
RV/PR8.6
mock/PVM.2
RV/PVM.2
mock/PVM.4
RV/PVM.4
mock/PVM.6
RV/PVM.6
B
RV/PR8.2
mock/PR8.2
RV/PR8.4
mock/PR8.4
RV/PR8.6
mock/PR8.6
RV/PVM.2
mock/PVM.2
RV/PVM.4
mock/PVM.4
RV/PVM.6
mock/PVM.6
C
PR8
PVM
Day
Contrast
RV v mock
PR8 v mock.0
RV/PR8 v mock.0
RV/PR8 v mock/PR8
PVM v mock.0
RV/PVM v mock.0
RV/PVM v mock/PVM

Fig 3

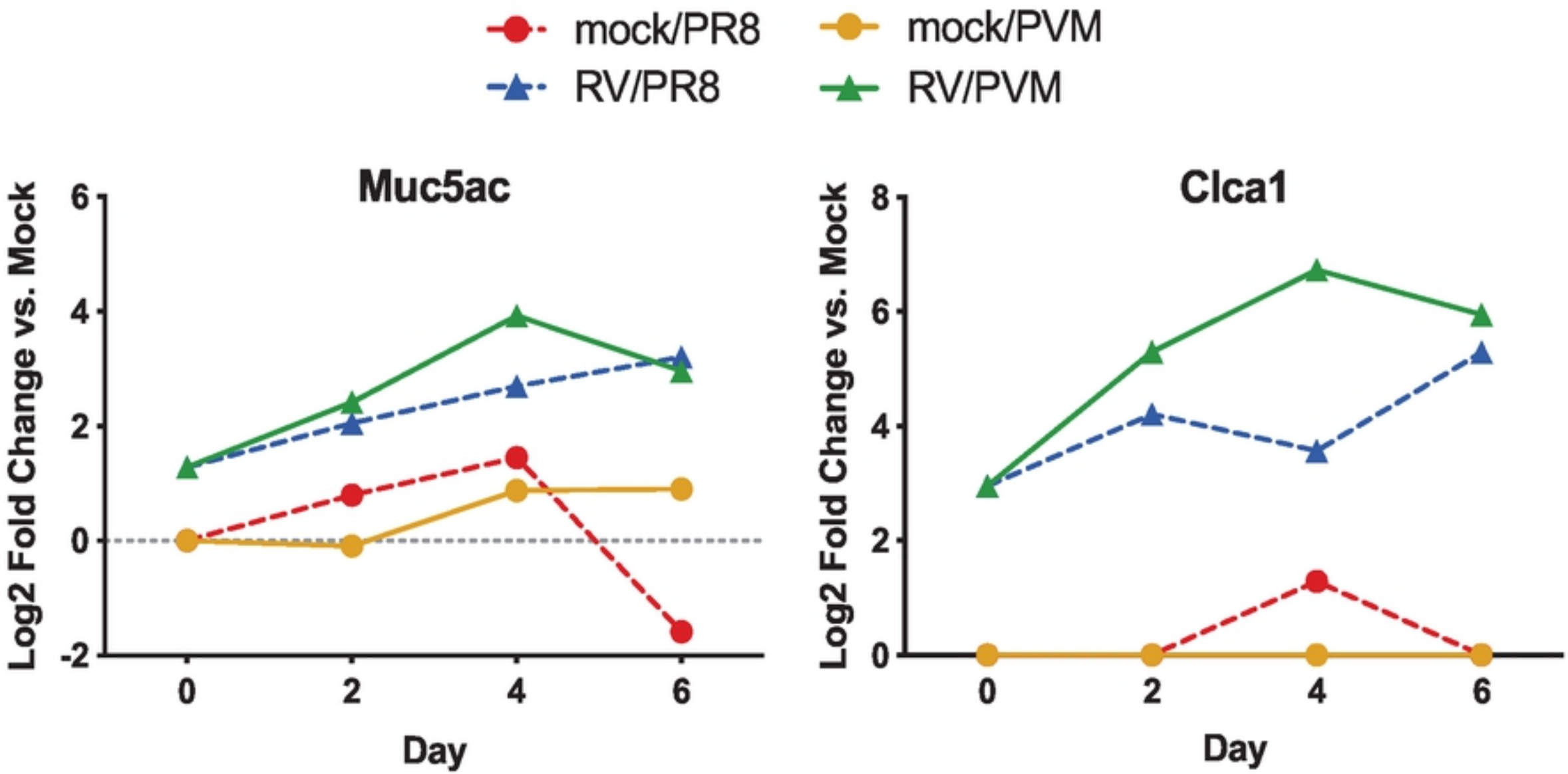
mock/PR8
mock/PVM
RV/PR8
RV/PVM
Muc5ac
Log2 Fold Change vs. Mock
6
4
2
0
-2
0
2
4
6
Day
Clca1
Log2 Fold Change vs. Mock
8
6
4
2
0
0
2
4
6
Day

Fig 5

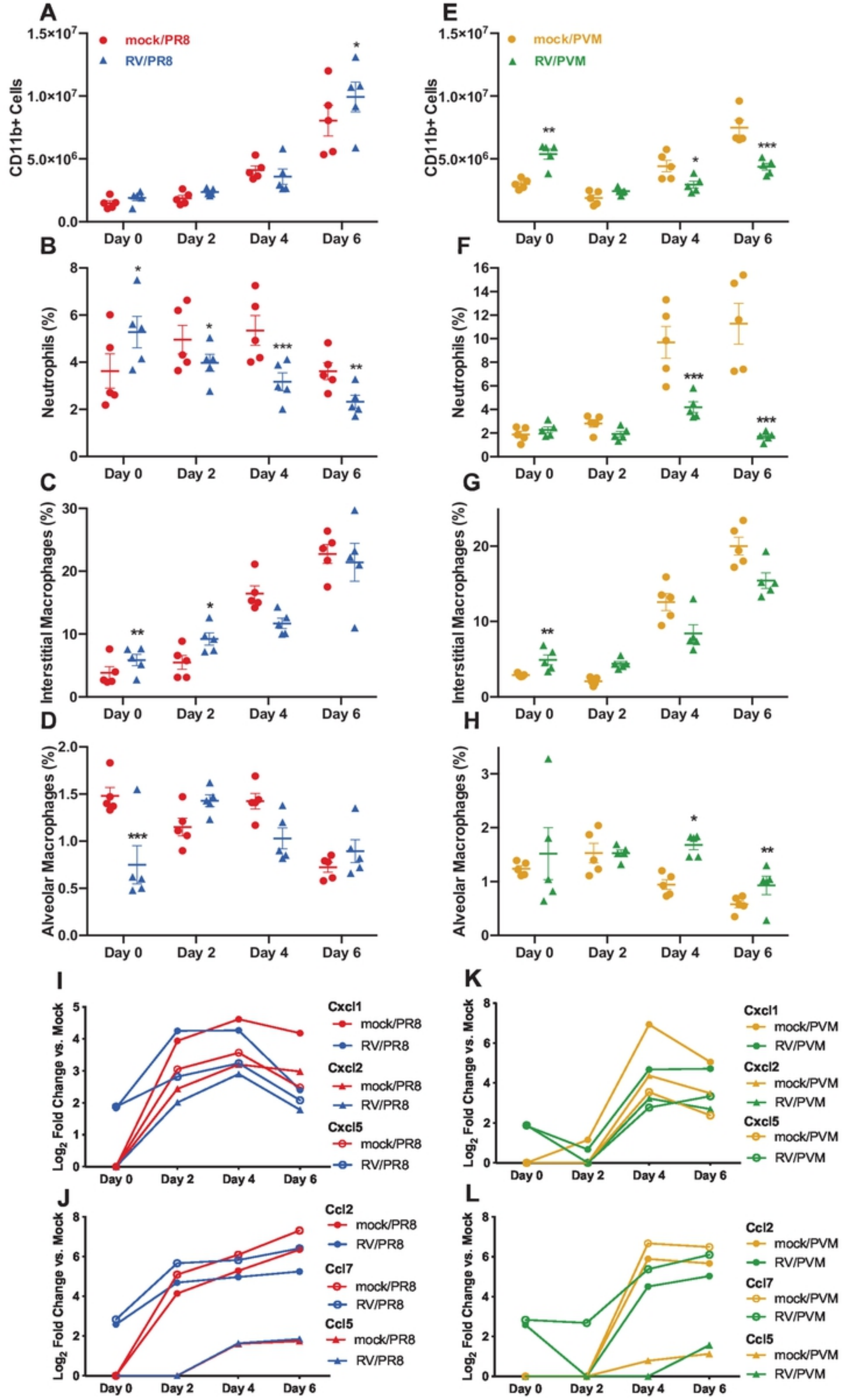
A
mock/PR8
RV/PR8
CD11b+ Cells
1.5×10^7
1.0×10^7
5.0×10^6
0.0
Day 0
Day 2
Day 4
Day 6
E
mock/PVM
RV/PVM
B
Neutrophils (%)
F
C
Interstitial Macrophages (%)
G
D
Alveolar Macrophages (%)
H
I
Log2 Fold Change vs. Mock
Cxcl1
Cxcl2
Cxcl5
K
J
Ccl2
Ccl7
Ccl5
L

Fig 7

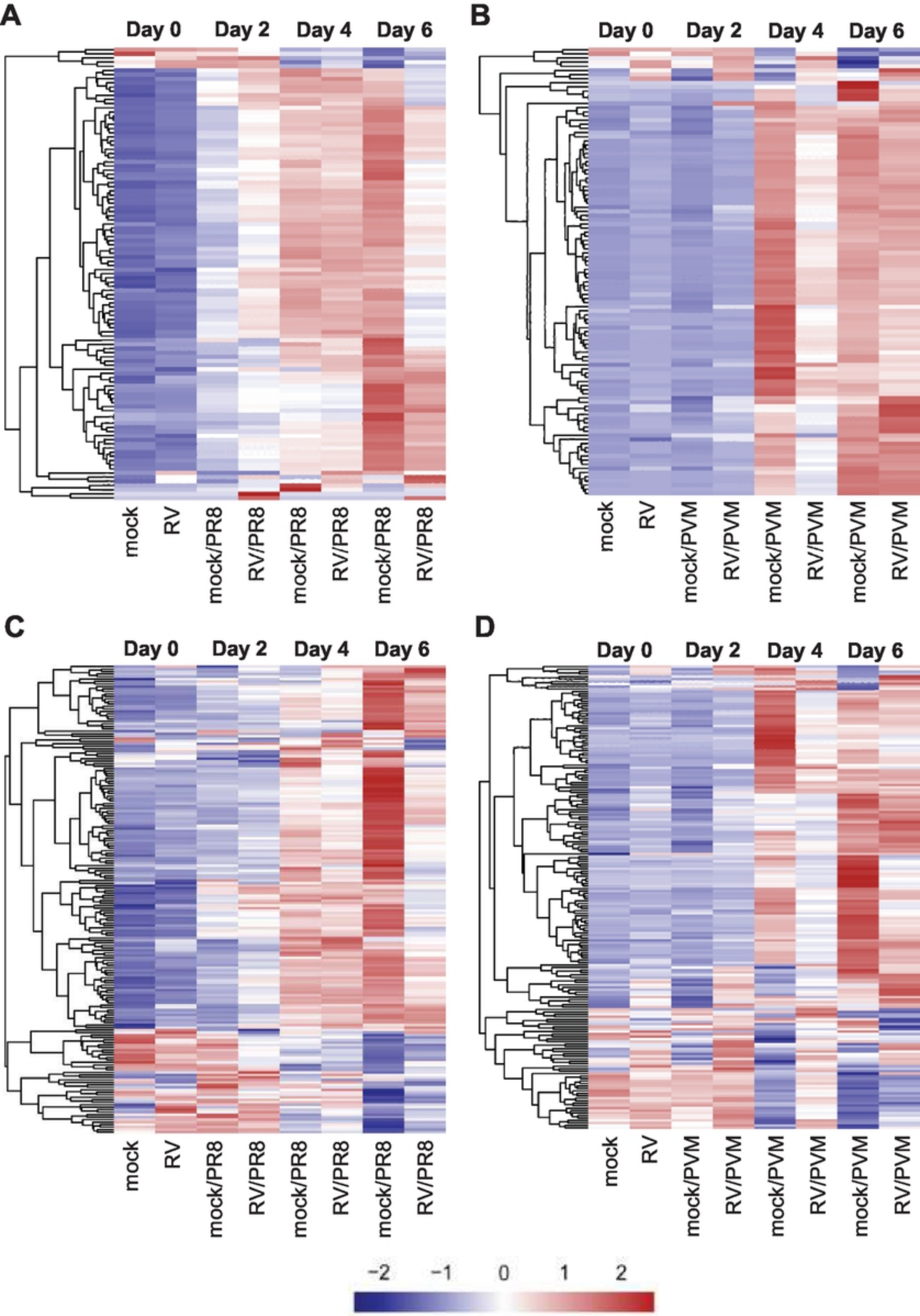
A
Day 0
Day 2
Day 4
Day 6
mock
RV
mock/PR8
RV/PR8
mock/PR8
RV/PR8
mock/PR8
RV/PR8
B
Day 0
Day 2
Day 4
Day 6
mock
RV
mock/PVM
RV/PVM
mock/PVM
RV/PVM
mock/PVM
RV/PVM
C
Day 0
Day 2
Day 4
Day 6
mock
RV
mock/PR8
RV/PR8
mock/PR8
RV/PR8
mock/PR8
RV/PR8
D
Day 0
Day 2
Day 4
Day 6
mock
RV
mock/PVM
RV/PVM
mock/PVM
RV/PVM
mock/PVM
RV/PVM
-2
-1
0
1
2

Fig 6

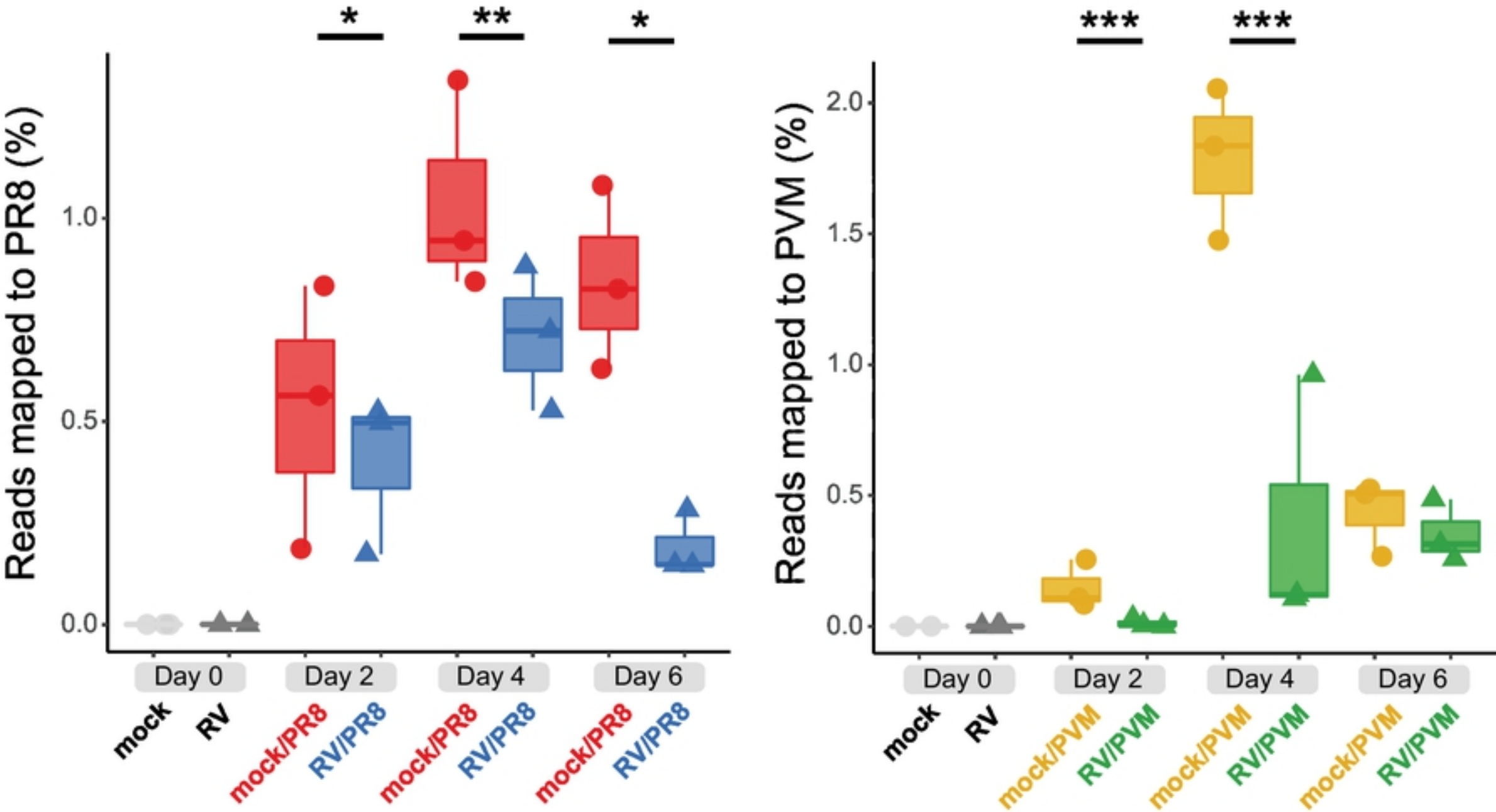
*
**
*
Reads mapped to PR8 (%)
1.0
0.5
0.0
Day 0
Day 2
Day 4
Day 6
mock
RV
mock/PR8
RV/PR8
mock/PR8
RV/PR8
mock/PR8
RV/PR8
***
***
Reads mapped to PVM (%)
2.0
1.5
1.0
0.5
0.0
Day 0
Day 2
Day 4
Day 6
mock
RV
mock/PVM
RV/PVM
mock/PVM
RV/PVM
mock/PVM
RV/PVM

Fig 4